Journal of Materials Chemistry

Cite this: J. Mater. Chem., 2012, 22, 21420

www.rsc.org/materials

PAPER

Facile synthesis of SiO_2–Au nanoshells in a three-stage microfluidic system

Leyre Gomez,[a] Manuel Arruebo,*[ab] Victor Sebastian,[ab] Laura Gutierrez[c] and Jesus Santamaria*[ab]

Received 28th June 2012, Accepted 28th August 2012
DOI: 10.1039/c2jm34206e

The capacity to produce nanostructured materials with well-defined, specific properties in relatively large quantities is crucial for the viability of emerging nanotechnologies. Core–shell plasmonic structures, such as SiO_2–Au nanoshells, are a type of nanomaterial where the control of morphological properties is especially important, given the strong dependence of the plasmon frequency on their characteristic dimensions. Here we present a simple, robust and scalable process to exploit the advantages of microfluidics to manufacture these sophisticated nanostructures. We show that the main sequential steps required to obtain SiO_2–Au nanoshells can be carried out in a simple microfluidic system with significant savings in time and effort, and with an improved control over the product properties, compared to a conventional batch processing operation.

1. Introduction

The properties of nanomaterials are critically dependent on their characteristics at the nanoscale, such as size, shape, surface composition and charge. Achieving homogeneity in product properties presents a serious challenge to current laboratory synthesis methods, generally based on batch processing, since, as recently noted[1] batch syntheses tend to suffer from irreproducibility of size, size distribution and quality of the produced nanomaterials. The lack of product homogeneity in batch systems has been attributed to factors such as inefficient mixing of reactants, and to the development of composition and or temperature gradients during reaction.[2]

Plasmonic structures such as nanoshells are a type of nanomaterial where control of morphological properties is especially important. Thus, in the case of SiO_2–Au core–shell structures, it has been shown that the resonant frequency of surface plasmon peaks can be tuned by controlling the ratio of shell thickness to particle diameter,[3] and in general the plasmonic properties of nanoshells are extremely sensitive to morphological variations.[4] Silica–gold nanoshells, first reported by Halas and co-workers,[3] have a high potential in biomedicine thanks to their biocompatibility and tunable optical properties in the near-infrared (NIR) region where body tissues and water present minimal absorption.[5] However, while most applications of nanoshells are focused on photothermal cancer therapy[6] other applications have been proposed, including surface-enhanced Raman scattering (SERS),[7] drug delivery,[8,9] waveguiding[10] and nanoprobes for sensing[11] and diagnosis.[12]

Given the critical dependence of plasmonic properties on the relative dimensions of the core and shell in SiO_2–Au structures, it is not surprising that considerable effort has been made to fine-tuning the variables of the synthesis process.[13–15] In spite of this, the synthesis remains a complex multi-stage process (synthesis of the silica cores, functionalization of their surface, synthesis of gold seeds, attachment of gold seeds to the core surface, growth of the seeds to form a continuous layer), whose result often varies according to the skills of the operator. Additional constraints refer to the need to produce such nanostructures in relatively large quantities with uniform sizes and well-defined characteristics and the ability to implement production on demand, in order to avoid long storage periods that may induce changes in product properties due to aggregation or to chemical changes. It seems clear that avoiding the inherent discontinuity of batch processing by operating at a steady state would improve product homogeneity and facilitate process scale-up.[16]

Microscale reactor systems can help to achieve these objectives[1,17] thanks to their small channel dimensions that provide a large surface area per unit of reactor volume and short diffusion lengths, resulting in fast mass and heat transport processes. Because of this, microreactors have become attractive systems in nanoparticle synthesis, including core–shell nanostructures such as CdSe/ZnS,[18] Au/Ag,[19] SiO_2/TiO_2,[20] ZnS/CdSe/Zn/S[21] or Au/Ag/Au.[22] Recently, Duraiswamy and Khan[23] reported the synthesis of SiO_2–Au plasmonic structures in a microreactor with segmented flow. In their work, pre-seeded silica nanoshells were mixed with a reductant and a gold plating solution in aqueous liquid cells, and an inert gas was used to create a string of gas and liquid compartments flowing along the reactor microchannels in immiscible silicone oil. With this 3-phase arrangement, they were

[a]Department of Chemical Engineering, Aragon Institute of Nanoscience (INA), University of Zaragoza, Campus Río Ebro-Edificio I + D, C/Poeta Mariano Esquillor S/N, 50018-Zaragoza, Spain. E-mail: Jesus.Santamaria@unizar.es; arruebom@unizar.es
[b]CIBER de Bioingeniería, Biomateriales y Nanomedicina (CIBER-BBN), Campus Río Ebro-Edificio I + D, C/Poeta Mariano Esquillor S/N, 50018-Zaragoza, Spain
[c]Institute of Catalysis and Petrochemistry–INCAPE-(FIQ,UNL-CONICET), Santiago del Estero 2829, 3000 Santa Fe, Argentina

able to control the degree of growth of the Au seeds on the silica surface, until a shell with the desired plasmonic properties was formed. The degree of growth of the gold structures was tunable and remarkably uniform, in contrast with batch synthesis experiments, where multimodal particle size distributions were obtained.

In this work we demonstrate that it is possible to use a single phase, non-segmented reactor arrangement to carry out this process. We have deliberately kept the process as simple as possible, using easily accessible laboratory hardware and straightforward arrangements, the only less usual piece of equipment being a commercial interdigital micromixer. The aim of this work is to prove that even a simple microreactor system presents significant advantages when sophisticated nanomaterials (such as gold nanoshells on silica cores) are to be obtained. We show that not only the growth of the seeded silica particles into a shell, but also the formation of the silica cores, their functionalization with amino groups and the attachment of the gold seeds to the functionalized silica surface can be carried out in the microreactor system developed, with significant savings in time and effort, and with an improved control over the product properties.

2. Experimental

2.1 Microreactor processing

The 3 stages of the synthesis process and the reactor setup are schematised in Fig. 1a. In each of the process stages, the reactants were instantaneously mixed using a commercial slit interdigital microstructured mixer from IMM (Institut für Mikrotechnik Mainz GmbH, Germany), and the desired reaction time was achieved by adjusting the length of a 1.3 mm internal diameter Teflon tubing, see Fig. 1b and c. Both the micromixer and the reaction tube were immersed in a thermostatic bath to control the reaction temperature. The reactants were fed into the micromixer using two syringe pumps (KD Scientific Inc. model KDS100) set at a rate of 4.7 mL h^{-1}. The special design of the micromixer (see Fig. 1c) divided the feeds into 15 channels of 40 microns that were merged at the outlet, achieving instant mixing by multi-lamination, focussing and subsequent volume expansion, which speeds up liquid mixing of the multi-lamellae and leads to jet mixing. The residence time was calculated as the ratio of the reactor volume (including the volume of the micromixer and the tubing) to the total volumetric flow rate, see Table 1.

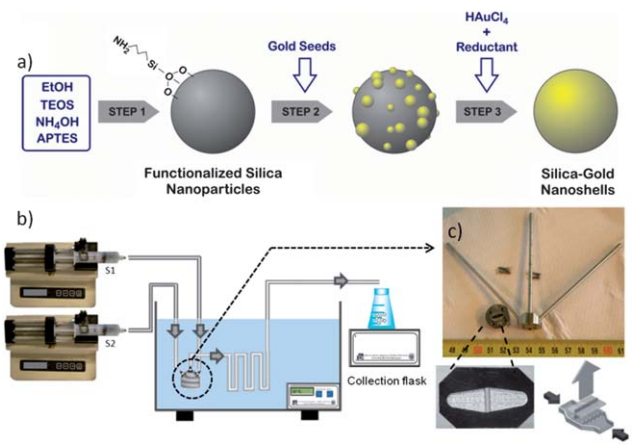

Fig. 1 (a) Diagram showing schematically the three stages of the process: synthesis of amino-functionalized silica nanoparticles, seeding with Au nanoparticles, shell formation. (b) Schematic from the experimental set-up for the continuous SiO_2–Au nanoshells synthesis. (c) Optical image of the opened micro-mixer (in the image the mixer is opened in two halves), the left-bottom inset is a detailed image of the bottom half showing the interdigital channels at both sides of the central slit from where the mixed products come out. Both inlet streams are divided into 16 sub-streams and recombined in order to increase the contact area between the reactants causing diffusion to occur faster. The right-bottom inset is a scheme of the flow arrangements inside the mixer. By thinning the multilamellae flow the mixing speed increases.

The first step in the synthesis was the formation of the silica nanoparticles used as cores. This was based on the well-known Stöber process[24] but we modified the process to obtain amino-functionalized silica nanoparticles as a product. Using absolute ethanol as solvent, an ammonium hydroxide solution was placed in one of the syringe pumps while tetra-ethyl orthosilicate (TEOS) and 3-aminopropyltriethoxy-silane (APTES) were placed in the other. Both mixtures were fed into the micromixer and the residence time in the microreactor immersed in the thermostatic bath (40 °C) was set to 30 minutes, see Table 1. The white product collected was centrifuged 3 times at 10 000 rpm for 10 minutes and then redispersed in ethanol under sonication. This process was necessary to remove excess APTES since we observed that its presence led to nanoparticle agglomeration caused by the interparticle hydrogen bonding between the surface silanol groups and the amine groups.[25] For comparison, the same process was carried out in a batch reactor using an agitated vessel (100 mL volume) at 25 °C, feeding TEOS into a solution of ethanol and ammonium hydroxide, while stirring for 1 hour. Then, the silica nanoparticle surface was functionalized feeding APTES while stirring for 2 hours at 25 °C plus one additional hour at 65 °C, see conditions in Table 1.

The objective of the second stage of the synthesis process was to obtain Au-seeded silica nanoparticles. To this end, gold nanoparticle seeds (2–4 nm) were synthesized and then attached to the amino-functionalized silica surface. The synthesis of the gold seeds was carried out separately by reducing a chloroauric solution with tetrakis(hydroxymethyl)phosphonium chloride (THPC), following the procedure described by Duff *et al.*[26] The Au nanoparticle seeds were dispersed in water at a pH around 2.5 (adjusted by adding HCl) and loaded in one of the syringe pumps, while the suspension of amino-functionalized silica nanoparticles was loaded in the other. As previously, the bath temperature and the residence time were fixed at 40 °C and 30 min, respectively (see Table 1). The product collected was centrifuged 3 times at 3500 rpm for 15 min and then redispersed in water, giving a reddish colour. In the case of batch processing, 1 mL of the amino-functionalized silica nanoparticles was manually shaken in contact with an excess of Au nanoparticle seeds (10 mL) with a pH adjusted at 2.5, and the mixture was allowed to settle for 2 hours at room temperature, see Table 1. The product was centrifuged until achieving a clear supernatant (at least 6 times) at 2000 rpm for 30 minutes and redispersed in 5 mL of water.

The last step of the synthesis was the growth of the gold shell from the Au nanoseeds deposited on the silica nanoparticles. In

Table 1 Synthesis conditions required in microreactor and batch reactor systems to obtain SiO_2–Au nanoshells. Reactants on streams S_1 and S_2, flow rates (Q_1, Q_2), reaction temperature (T) and residence time (t_R) for each of the three stages in the process[a]

Microreactor					
Step	T^a, °C	t_R, min	Flows, mL h^{-1} Q_1, Q_2	Reactants on stream S_1	Reactants on stream S_2
1	40	30	5	EtOH + TEOS + APTES	EtOH + NH_4OH
2	40	30	5	EtOH + Product 1	H_2O + HCl + Au seeds
3	25	5	5	Product 2 + Formaldehyde	$HAuCl_4$ and K_2CO_3 solution

Batch reactor		
Step	T^a, °C	t_{rc}, min
1	25	60
Functionalization	25|65 °C	120 + 60
2	25	120
3	25	5

[a] t_R: residence time, t_{rc}: reaction time, S_1 and S_2: syringe located in pump 1|2, Q_1 and Q_2: flow rate in pump 1|2, T: reaction temperature.

this case, one of the syringes was loaded with a gold solution containing $HAuCl_4$ and K_2CO_3 prepared as described in the literature.[27] The other syringe contained the Au-seeded silica nanoparticles and formaldehyde as the reduction agent. This process was carried out at 25 °C and 5 min residence time, see Table 1. To carry out the same process in the batch reactor, 4 mL of the reductant solution with $HAuCl_4$ were placed in a 10 mL round flask containing 200 μL of the Au-seeded silica nanoparticles. While stirring at 25 °C, 10 μL of formaldehyde were fed. After 5 minutes, the gold shell around the silica nucleus was completed. For each of the 3-stages an initial work was carried out in order to optimize the flow rates and tubing diameters to achieve specific Reynolds numbers (around 500), under laminar flow regime, which rendered nanoparticles with the required characteristics (monodispersity and SPR absorbance in the NIR region).

2.2 Nanoparticle and nanoshell characterization

The produced nanoparticles were characterized either as dry powders or as aqueous dispersions using a battery of techniques. Particle size distributions were obtained from scanning electron microscopy, SEM (FEI Instruments model Inspect F) for the silica nanoparticles of the first stage and from transmission electron microscopy (TEM) (FEI Tecnai T20, operated at 200 kV) for the Au seeds. Occasionally the presence of agglomerates was checked using dynamic light scattering, DLS (90 Plus, Brookhaven Instruments Corp.). The same instrument also provided the Z-potential of the nanoparticle dispersions as a function of pH. The appearance of the silica particles as they were progressively covered by gold (from the initial seeding to the fully grown shell) was generally followed with a higher resolution TEM (FEI TECNAI F30, operated at 300 kV).

The functionalization of the silica surface with amino groups was followed by Fourier transform infrared (FTIR) spectroscopy using a Bruker Vertex 70 FTIR spectrometer. The extinction spectra of the SiO_2–Au nanoparticles and of the Au nanoparticle seeds were measured in a UV-visible-NIR spectrophotometer (V-67, Jasco Company).

3. Results and discussion

Fig. 2a shows the characteristics of the product obtained from the microreactor after the first synthesis stage. The SEM view shows the expected result from a Stöber-type synthesis of silica nanoparticles: population of well-dispersed nanoparticles, with a homogeneous appearance. In spite of this, it should be noted that there is some scatter in the particle size distribution (79 ± 19 nm, see Fig. 2b), which is likely a consequence of the residence time distribution of the fluid elements in the reactor. Although the initial mixing is instantaneous, the flow in the reaction tube takes place in the laminar regime ($Re \ll 2100$), meaning that a pronounced radial velocity profile develops, with the corresponding difference in residence times for the fluid elements at different radial positions. While this could be corrected by using a slug flow to obtain a uniform residence time,[1] the objective of this work is to produce Au nanoshells while keeping the system as simple as possible, and involving a second gas or liquid phase would introduce undesired complexity in the system design and operation. Fig. 2c also shows the FTIR spectra of the amino-functionalized silica nanoparticles obtained in microreactor and batch reactor. It can be seen that in both cases the functionalization has been successful and the characteristic peaks of $–CH_2$ and $–CH_3$ stretching vibrations attributed to the aminosilanes are shown at around 2800–3000 cm^{-1} (bands at 2955 and 2925 cm^{-1} characteristic of the asymmetric CH_3 stretching and the symmetric CH_2 stretching, respectively).

Seeding of the amino-functionalized silica shells was also carried out efficiently in the microreactor system, thanks to a careful control of the reaction conditions, and particularly the pH. A population of Au seeds with a narrow particle-size distribution (Fig. 3a) was continuously fed to one inlet of the micromixer, while the other provided a steady flux of the amino-functionalized silica nanoparticles. Fig. 3b shows the variation of the Z-potential of the Au and amino-functionalized silica nanoparticles as a function of pH. It can be seen that the Au seeds present a roughly constant charge around −20 mV, while there is a strong variation in the charge of the silica nanoparticles, which have an isoelectric point at around

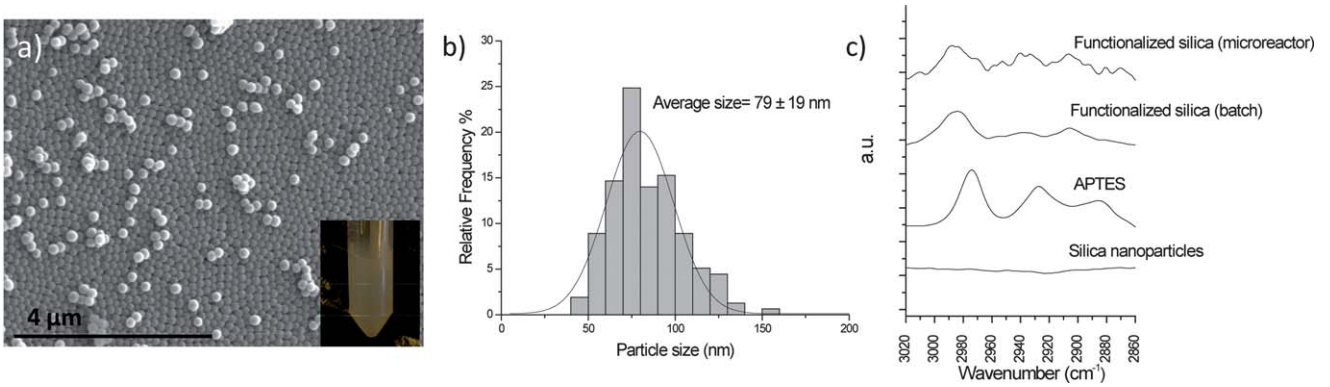

Fig. 2 (a) SEM view of the amino-functionalized silica nanoparticles produced in the first stage of the process using a microreactor (inset: appearance of the nanoparticle suspension). (b) Particle size distribution obtained from analysis of the SEM pictures ($N > 200$). (c) FTIR spectra of the amino-functionalized product nanoparticles obtained in batch and microreactor systems. The patterns corresponding to APTES and to non-functionalized silica are also shown for comparison.

pH = 5. When seeding was carried out at pH = 6.5 (Fig. 3c) seeding was non-uniform, with agglomeration of the Au seeds and large bald areas on the silica nanoparticles. On the other hand, at pH = 2.5 the silica is positively charged (around +50 mV), and the electrostatic attraction leads to a uniform distribution of well-dispersed gold nanoparticles (Fig. 3d and e). A few Au seed agglomerates can be seen between the particles (Fig. 3d), but the vast majority of the seeds are homogeneously distributed on the amino-functionalized silica surface. This is in contrast with the results found in the batch reactor (Fig. 3f) where, while the silica surface is also efficiently seeded, many loose Au agglomerates can be identified. The presence of unattached Au nanoparticles is likely a result of a less effective mixing in the batch reactor. Electrostatic attraction favours

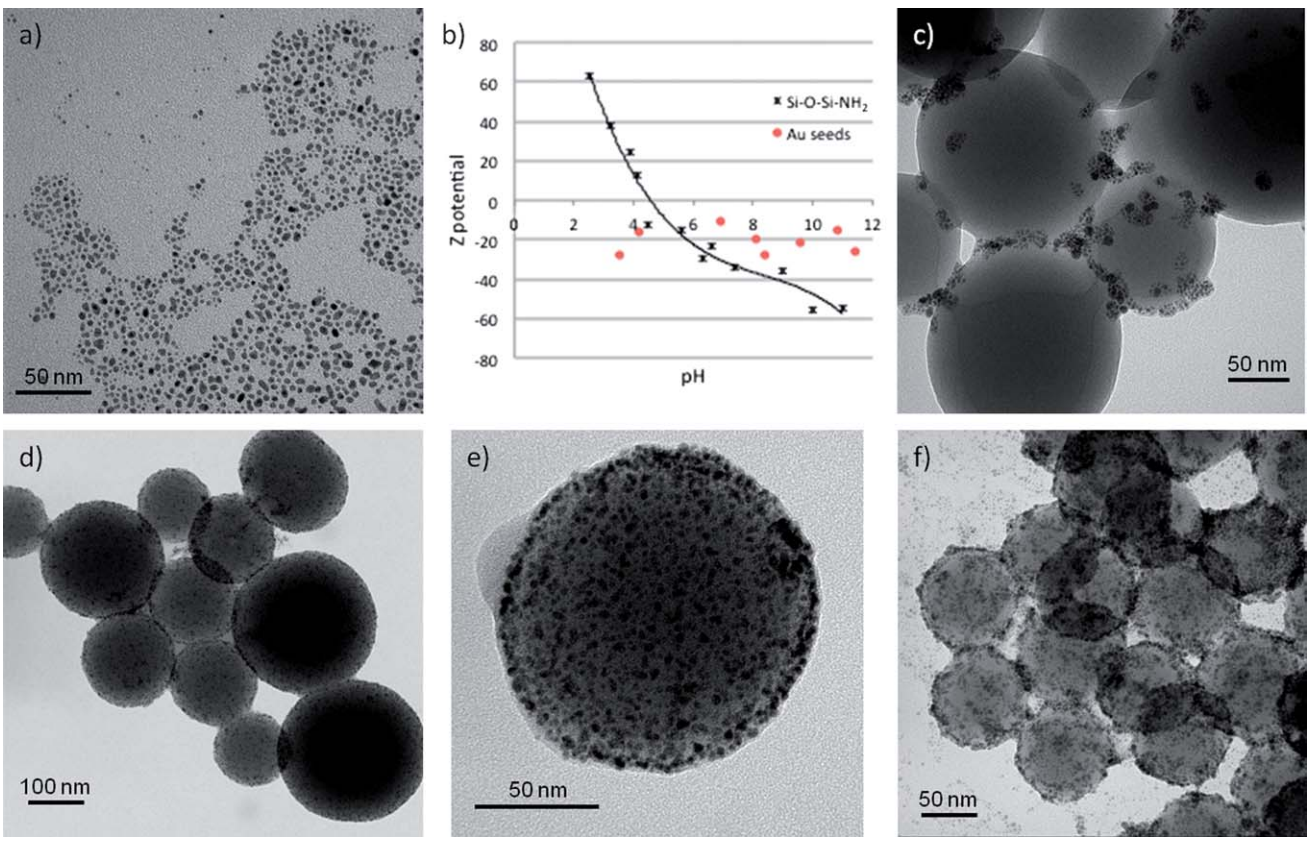

Fig. 3 Characterization of the seeding stage. (a) TEM view of the gold seeds used. (b) Variation of *Z*-potential with pH for the Au seeds and the amino-functionalized silica nanoparticles. (c) TEM view of Au-seeded silica nanoparticles at pH = 6.5 (microreactor). (d) TEM view of Au-seeded silica nanoparticles at pH = 2.5. (e) Close up TEM view of a Au-seeded silica nanoparticle at pH = 2.5 (microreactor). (f) TEM view of Au-seeded silica nanoparticles at pH = 2.5 (batch).

attachment of the Au seeds, and this is easily achieved in the microreactor system, since the seeds and the silica nanoparticles are brought into close contact in the micromixer. On the other hand, if mixing is less efficient, there is a chance that Au seeds do not come into contact with the silica particles, remaining unattached or even forming agglomerates among themselves, as shown in Fig. 3f. The presence of unattached Au nanoparticles presents two main problems. First, their removal is challenging and it cannot be fully guaranteed, even after the laborious centrifugation–washing procedure used in this work, as discussed below. Second, the non-attached gold represents a waste of Au seeds. In fact, to guarantee a good coverage of Au seeds on the silica surface, the original recipe[27] called for 10 mL of Au nanoparticles solution with 1 mL silica nanoparticles. In the microreactor we have been able to reduce this ratio to 2 : 1 and still obtain a good coverage without apparent bald spots, as shown in Fig. 3e.

The last stage in the nanoshell synthesis involved the growth of the Au seeds to form a gold shell. To this end, the seeded nanoparticles plus formaldehyde were fed to one inlet of the micromixer and the Au precursor ($HAuCl_4$) to the other. Fig. 4 shows some representative examples of the product obtained in the microreactor and in the batch system. In both cases a good shell growth is obtained, as can be seen in the closer images of Fig. 4b and c. This is reflected in the absorption spectra of Fig. 5a and b, where a clear plasmon is observed for both types of nanoshells, with intense absorbance in the 700–900 nm wavelength range. However, a closer examination of the TEM micrographs in Fig. 4a and d show additional differences. In the case of the Au nanoshells prepared in the microreactor (Fig. 4a) almost all of the gold is attached to the silica surface. Only a few non-integrated nanoparticles may be spotted (see arrows in Fig. 4d), and even these are close to the edges of the particles and seem to be attached. This is in contrast with the nanoshells prepared in the batch system, where significant concentrations of loose nanoparticles can be observed (Fig. 4d). These likely originate from the growth of non-attached Au nanoseeds thanks to the $HAuCl_4$ added in the third stage, allowing them to reach sizes of 10 nm and larger.

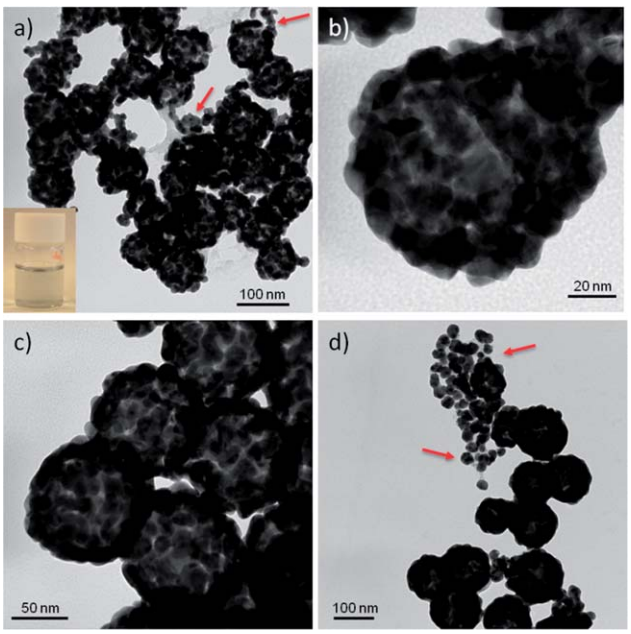

Fig. 4 TEM views of fully grown nanoshells obtained in microreactor (a and b) and batch reactor (c and d) systems. The appearance of the nanoshell suspension is shown as an inset in (a).

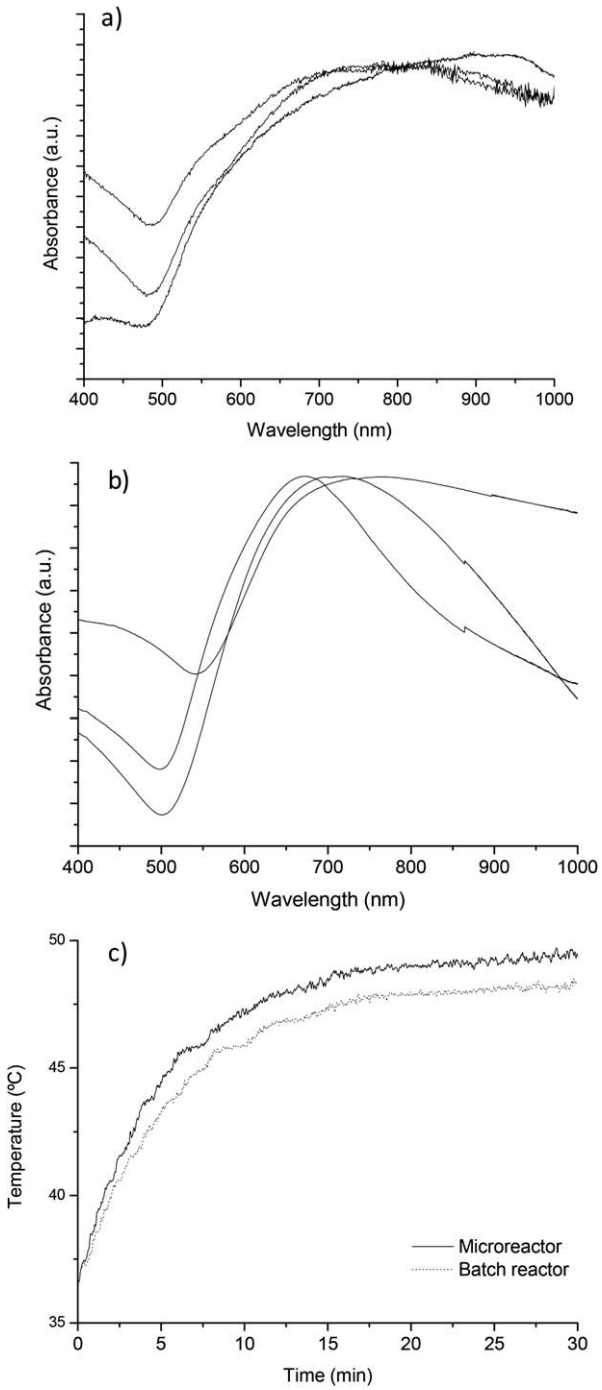

Fig. 5 Reproducibility of optical absorption spectra for nanoshells prepared in three independent batches in (a) microreactor and (b) batch reactor. (c) An example of the heating profiles obtained when suspensions of nanoshells prepared in both reaction systems (concentration of 0.1 mg nanoshells per mL) were irradiated with a continuous 808 nm laser system (at a power of 2 W).

The influence of these loose Au nanoparticles can be observed in the absorption spectra of Fig. 5b, where the blue shift plasmon displacement can be explained as a consequence of the contribution to the total absorption of these loose nanoparticles. These loose nanoparticles have a direct effect on the reproducibility of absorption spectra. Their presence and concentration depend on the success of the washing cycles after stage 2, whose effectiveness is difficult to be guaranteed, given the small size of the seeds. As a consequence, the absorption spectra of the nanoshells prepared in the batch reactor present more variability, considering the position of the maxima and the width of the plasmon band. While the effect on the heating is moderate (Fig. 5c indicates that the heating rates obtained with shells prepared in the microreactor and batch reactor are similar), the absorption spectra obtained with the nanoshells prepared in the microreactor are more reproducible and closer to 800 nm. Another potential explanation of this blue shift could be attributable to thicker shell thicknesses in the nanoparticles produced using the batch reactor compared to the ones obtained for the micromixer-produced nanoparticles; however, both thicknesses were statistically measured and their averaged data did not show significant differences.

4. Conclusions

A simple microreactor device provides an efficient platform to perform the three main processes involved in the formation of SiO_2–Au nanoshells (synthesis and functionalization of the silica cores, seeding with Au nanoparticles and growth of Au seeds to form Au shells). Some variation in the final nanoshell size is obtained as a consequence of the particle size distribution of the silica cores, which in turn caused by the radial velocity profiles leading to a range of reaction times in the first reaction stage. In spite of this, nanoshells with suitable plasmonic properties were obtained, with good reproducibility. The synthesis can be carried out continuously and in a controlled manner, provided that a fast mixing of the reactants is achieved in each stage. By comparison, the same process carried out in a batch reactor system was considerably more expensive in terms of time, labour and reactants, and led to a more heterogeneous product. Furthermore, this approach makes it feasible to produce nanoshells on demand at the point of need which is highly desirable for numerous applications in nanoscale science and technology.

Acknowledgements

This work has been supported thanks to the Spanish Ministry of Science and Innovation (MICINN) for the MAT2011-24988 grant. Funding from Fundación Ramón Areces (Spain) and from ERC Advanced Grant (ERC-AdG-Grant Agreement No 267626, HECTOR) is gratefully acknowledged.

Notes and references

1 S. Marre and K. F. Jensen, *Chem. Soc. Rev.*, 2010, **39**, 1183.
2 L. Gutierrez, L. Gomez, S. Irusta, M. Arruebo and J. Santamaria, *Chem. Eng. J.*, 2011, **171**, 674.
3 S. J. Oldenburg, R. D. Averit, S. L. Westcott and N. J. Halas, *Chem. Phys. Lett.*, 1998, **288**, 243.
4 M. Hu, *Chem. Soc. Rev.*, 2006, **35**, 1084.
5 R. Weissleder, *Nat. Biotechnol.*, 2001, **19**, 316.
6 D. P. O'Neal, L. R. Hirsch, N. J. Halas, J. D. Payne and J. L. West, *Cancer Lett.*, 2004, **209**, 171.
7 H. Wang, J. Kundu and N. J. Halas, *Angew. Chem., Int. Ed.*, 2007, **119**, 9198.
8 M. Bikram, A. M. Gobin, R. E. Whitmire and J. L. West, *J. Controlled Release*, 2007, **123**, 219.
9 C. Yague, M. Arruebo and J. Santamaria, *Chem. Commun.*, 2010, **46**, 7513.
10 S. Lal, S. Link and N. J. Halas, *Nat. Photonics*, 2007, **1**, 641.
11 B. B. Xu, X. Y. Ma, Y. Y. Rao, J. Dong and W. P. Qian, *Chin. Sci. Bull.*, 2011, **56**, 3234.
12 A. Agrawal, S. Huang, A. W. H. Lin, M. H. Lee, J. K. Barton, R. A. Drezek and T. J. Pfefer, *J. Biomed. Opt.*, 2006, **11**, 041121.
13 S. L. Westcott, S. J. Oldenburg, T. R. Lee and N. J. Halas, *Langmuir*, 2008, **14**, 5396.
14 N. Phonthammachai, J. C. Kah, G. Jun, C. J. Sheppard, M. C. Olivo, S. G. Mhaisalkar and T. J. White, *Langmuir*, 2008, **24**, 5109.
15 B. E. Brinson, J. B. Lassiter, C. S. Levin, R. Bardhan, N. Mirin and N. J. Halas, *Langmuir*, 2008, **24**, 14166.
16 C. H. Chang, B. K. Paul, V. T. Remcho, S. Atre and J. E. Hutchison, *J. Nanopart. Res.*, 2008, **10**, 965.
17 C. X. Zhao, L. He, S. Z. Qiao and A. P. J. Middelberg, *Chem. Eng. Sci.*, 2011, **66**, 1463.
18 H. Wang, X. Li, M. Uehara, Y. Yamaguchi, H. Nakamura, M. Miyazaki, H. Shimizu and H. Maeda, *Chem. Commun.*, 2004, 48.
19 J. M. Köhler, H. Romanus, U. Hübner and J. Wagner, *J. Nanomater.*, 2007, 98134.
20 S. A. Khan and K. F. Jensen, *Adv. Mater.*, 2007, **19**, 2556.
21 M. Uehara, H. Nakamura and H. Maeda, *J. Nanosci. Nanotechnol.*, 2009, **9**, 577.
22 A. Knauer, A. Thete, S. Li, H. Romanus, A. Csáki, W. Fritzsche and J. M. Köhler, *Chem. Eng. J.*, 2011, **166**, 1164.
23 S. Duraiswamy and S. A. Khan, *Nano Lett.*, 2010, **10**, 3757.
24 W. Stöber and A. Fink, *J. Colloid Interface Sci.*, 1968, **26**, 62.
25 J. Lu, M. Liong, J. I. Zink and F. Tamanoi, *Small*, 2007, **3**, 1341.
26 D. G. Duff, A. Baiker and P. P. Edwards, *Langmuir*, 1993, **9**, 2301.
27 T. Pham, J. B. Jackson, N. J. Halas and T. R. Lee, *Langmuir*, 2002, **18**, 4915.